Structural Studies of Extension-Induced Mesophase Formation in Poly(diethylsiloxane) Elastomers: In Situ Synchrotron WAXS and SAXS

Hilmar Koerner,† Yixia Luo, Xuefa Li, Claude Cohen,* Ronald C. Hedden,‡ and C. K. Ober

School of Chemical and Biomolecular Engineering, Olin Hall, and Department of Materials Science and Engineering, Bard Hall, Cornell University, Ithaca, New York 14853

Received June 3, 2002

ABSTRACT: Amorphous poly(diethylsiloxane) (PDES) elastomers undergo a transition to an aligned mesomorphic state when subjected to uniaxial tension. The structural changes associated with this transition and the kinetics of its formation have been investigated by in-situ synchrotron wide-angle and small-angle X-ray scattering. In the mesomorphic state, the PDES elastomers are biphasic, consisting of aligned mesophase domains and amorphous material. Because of the well-defined structure of the networks used, we were able to determine that the mesophase domain size is governed by the precursor chain length and is unaffected by trapped entanglements. The observed increase in mesophase content with increase in extension ratio in a fully necked sample is caused by an increase in the number of mesophase domains rather than an increase in domain size. In the extended state, PDES elastomers attain a very high degree of segment orientation comparable to that of mesogen-containing liquid crystalline elastomers.

Introduction

The physical properties of elastomers that undergo a strain-induced phase transition from an amorphous state to an aligned mesomorphic state have attracted attention because these materials could potentially be applied in such devices as stress−optical switches, strain−temperature devices, or certain membrane applications.[1] Others have suggested the use of such elastomers as possible materials to model muscle tissue.[2] Spontaneous alignment under extension is typically exhibited by chemically complex cross-linked nematic liquid-crystalline polymer networks and is unusual for a pure homopolymer such as poly(diethylsiloxane) (PDES) with no obvious rigid "mesogens". The ability of PDES to form a mesophase appears to stem from the existence of multiple conformational isomers of similar energy that allows part of the chain to be rigid, with a flat backbone as in its crystalline phase, and part of it flexible as in its amorphous phase.[3] As in the case of isotactic polypropylene that also exhibits a mesophase due to different helical conformation in the crystalline structure,[4] the mesophase of PDES has been classified as a conformationally disordered (or *condis*) crystal.[5] We shall use the term mesophase throughout this article to mean conformationally disordered crystalline phase and shall use the tools developed for crystalline polymers to analyze the data from our samples.

An amorphous PDES network placed under uniaxial extension will form a "neck" at a moderate extension.[1,6] The neck region consists of a mixture of an aligned birefringent mesophase and an amorphous phase. Measurements of optical microscopy, dynamic mechanical analysis, and ^{2}H NMR spectroscopy have provided a clear picture of mesophase formation and orientation process in carefully synthesized PDES networks subjected to uniaxial extension. PDES networks subjected to uniaxial extension remain amorphous until a critical elongation when spontaneous alignment takes place, resulting in a contracted neck region of decreased cross-sectional area. The mesophase content and segment orientation in the neck region were recently probed by deuterium NMR at various extension ratios.[7] As the overall extension ratio of the sample is increased, the neck region grows at the expense of the single-phase amorphous regions on either side of the neck. The local extension ratio of both the neck and the single-phase amorphous region remain constant as the sample elongates by converting single-phase amorphous material in the transition region into the mesomorphic neck. Once the entire sample is necked, its mesophase content increases with the increase in the extension ratio through conversion of the amorphous material in the neck into the mesophase.[7]

X-ray scattering measurements and differential scanning calorimetry thermograms have been reported on PDES networks synthesized by random cross-linking of precursor chains using peroxide vulcanization[8] or by hydrosilylation end-linking of precursor chains.[9] In both these cases, the structure of the networks was not well characterized either due to the wide distribution of strand size between cross-links or due to imperfections caused by high soluble fractions. Nonetheless, the structure of the unit cell and its dimension in the mesophase were established to be identical to those observed in the mesophase of un-cross-linked high molecular weight PDES and similar to the monoclinic α_1 crystal phase present at low temperatures.[8] In the present work, the networks were formed from low polydispersity, low molar mass precursors that lead to amorphous samples when end-linked. We used in situ synchrotron wide-angle X-ray scattering (WAXS) and small-angle scattering (SAXS) from the mesophase formed by stretching these well-characterized PDES networks to address issues that have remained unresolved. In particular, is the increase in mesophase content in the fully necked sample caused by an increase

† Present address: Non-Metallic Division, University of Dayton Research Institute, Dayton, OH.

‡ Present address: NIST, Polymers Division, Gaithersburg, MD.

10.1021/ma020856j CCC: $25.00
Published on Web 02/27/2003

Table 1. Characteristics of PDES Samples[a]

sample	sample ID in ref 11 (Hedden et al.)	precursor M_n (kg/mol)	precursor M_w (kg/mol)	M_c (kg/mol)	d spacing of 110 (Å)	L (Å)
1	Opt-d_2-2c	19.9	24	12.8	7.73	270
2	Opt-4	20.8	25.4	12.6	7.80	260
3	Opt-2	25.7	32.8	13.5		295
4	Opt-1	34.5	48.7	13.1	7.94	380

[a] M_c is given by $\rho RT/G_e$, where ρ is the density of the polymer and G_e is the equilibrium elastic shear modulus of the network. L is calculated from SAXS.

of the extension ratio due to an increase in mesophase domain size or an increase in the number of domains that have a constant size? By using networks with well-defined structures, we are able to investigate the role of the structural parameters of the network on the mesophase domain size. Finally, we are also able to examine the kinetics of mesophase formation as determined from in situ SAXS measurements.

Experimental Procedures

Sample Preparation. Networks were prepared by hydrosilylation end-linking of telechelic precursor chains having vinyl ends with the tetrafunctional cross-linker tetrakis(dimethylsiloxy)silane. The synthesis of the precursors and the cross-linking procedure were described in earlier publications.[6] The soluble fractions extracted in toluene had values of about 1% or less, indicating that the networks can be considered as optimal with small amounts of defects.[10] The samples were cut out in the form of rectangular films of approximately 2 cm by 0.5 cm and a thickness of 1.25 mm. The samples used are listed in Table 1, and their elastic moduli were previously determined using a Perkin-Elmer DMA 7e in uniaxial extension at 25 °C at a strain of approximately 1%.[11] The values of M_c reported in Table 1 are the molar mass of elastic strands between effective cross-links and are obtained using the simple inverse relation between M_c and equilibrium shear modulus G_e of ideal rubber elasticity, $M_c = \rho RT/G_e$, where ρ is the density and R and T have their usual meaning.

X-ray Measurements. The measurements were carried out at the Cornell High Energy Synchrotron Source (CHESS) at the D1 beamline, using a wavelength of 1.41 Å. The initial beam was trimmed down with three slits to a width and height of about 200 μm. The sample-to-film distance for WAXS was set to 84 mm and for SAXS to 1333 mm. Images were collected with a CCD (charged couple device) camera that produced native 16 bit images. A Matlab routine was used to analyze the X-ray patterns. Because of an additional high-energy X-ray component, second harmonics were observed for intense Bragg reflections during X-ray diffraction experiments. As outlined in the Introduction, the goal of the X-ray experiments was not to characterize the structure of mesomorphic PDES, which is already established, but to understand the kinetics and morphological changes at the transition from the amorphous to the mesophase. Wide- and small-angle X-ray scattering (WAXS, SAXS) were used to study the structure as a function of position in the stretched samples and the time evolution of the mesophase upon elongation of the samples.

Extension Device. An aluminum extension device was used to stretch the samples in the beam. The PDES samples were mounted in between clamps. A caliper was used to measure the length of the sample under different stretch conditions. To obtain local extension ratios, ink dots were marked onto the sample and images taken at each extension ratio with a digital camera. Changes in distances between ink dots were analyzed to determine the local extension ratio α. It was found that when the sample was tightly clamped, preventing any slippage at the clamps during the experiments, and the entire sample is fully necked, the local extension ratio α along the length of the sample equaled the overall extension ratio of the entire sample. However, if the sample was partially necked, α varied along the sample with higher values in the neck and lower values in the amorphous region. Sample 3 was therefore scanned along the extension direction (x-axis) as well as in the transverse direction (z-axis), and WAXS patterns were taken about every 20 min over a period of 8 h. The sample was stretched by almost 3-fold and was immediately mounted on the sample stage for X-ray exposures at ambient temperature. Several points marked by ink dots were selected so that the development of the mesomorphic phase could be observed at some specified sample point. Exposures were taken at these ink dots as time evolved. Slight movements of these points would not affect the measurements since the beam size of X-ray is 200 μm, which turns out to be much larger than the size of domains detected by WAXD (~300 Å).

Data Analysis. To obtain a value for the extent of mesophase formation from the WAXS patterns, we applied the internal method that does not require a reference sample. Since X-ray diffraction gives distinct patterns for the mesophase and the amorphous phase, the diffraction from the mesophase and amorphous phase can be easily distinguished in general. If the background and the noise are subtracted, the diffraction intensity is essentially the superposition of the diffraction intensity from the mesophase, I_m, and the diffraction intensity from the amorphous phase, I_a. It is therefore natural to take the mesophase as the fraction of crystalline diffraction intensity[12]

$$\psi = I_m/(I_m + I_a) \tag{1}$$

It is important to note that percent of mesophase or crystallinity (as the case may be) of a given sample determined by different physical techniques may be different.[13] Fiber patterns of unoriented polymers show rings on the X-ray pattern. A characteristic feature of an oriented X-ray pattern is the formation of arcs. The azimuthal width of the arcs provides information about the degree of the orientation. A value for the degree of orientation was developed for three dimensions by Hermans and is called the Hermans orientation parameter. The orientation parameter is computed by integration of intensity along the azimuthal direction at a given 2θ value of a reflection. Background azimuthal scans at the same 2θ angle were subtracted after correcting for differences in incident flux. The distribution in intensity (I) as a function of the azimuthal angle (β) for a given quadrant of the azimuthal scan was obtained. Peaks in intensity were made to reside at an angle of $\beta = 90°$. Conversion of the $I(\beta)$ data to $I(\phi)$ is accomplished using the following relationship from spherical trigonometry

$$\cos(\beta)\cos(\theta_B) = \cos(\phi) \tag{2}$$

where θ_B is the Bragg angle and ϕ is the angle between the normal to the scattering plane (defined by the incident and scattered beams) and the stretching direction. Note that for moderate to small Bragg angles the angle of inclination of the plane normal to the uniaxial direction, ϕ, is practically equal to the azimuthal angle β as directly measured on the image. To calculate the average cosine squared of ϕ, integration of the $I(\phi)$ data vs ϕ is performed using eq 3

$$\langle \cos^2 \phi \rangle = \frac{\int_0^{2\pi} I(\phi)\cos^2(\phi)\sin(\phi)\,d\phi}{\int_0^{2\pi} I(\phi)\sin(\phi)\,d\phi} \tag{3}$$

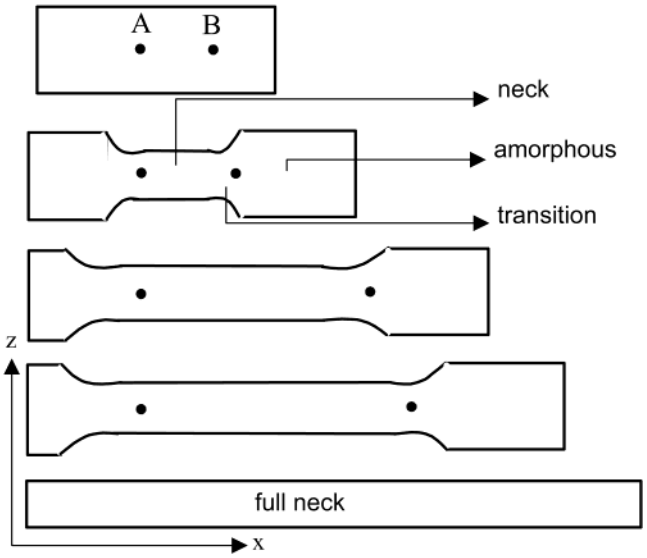

Figure 1. Neck formation upon elongation of elastomers (arbitrary scale).

The director orientation parameter, S_d, is then calculated using the Hermans orientation function:

$$S_d = \frac{3\langle\cos^2\phi\rangle - 1}{2} \tag{4}$$

Orientation parameters reported here are the averages of the four orientation parameters calculated from each quadrant. These were found to differ at most by 10% from each other.

We will assume that the well-accepted two-phase model for semicrystalline polymers by Hosemann[14] can be applied to the present siloxane system. Since the order in the mesophase is not high enough to form crystallites with well-defined three-dimensional order (diffuse scattering on WAXS patterns), the term "crystallites" in the Hosemann model has to be redefined as "domains" for the PDES system. Chains are oriented parallel to each other upon alignment (stretching) and form domains that are separated by amorphous regions. If the domains are of uniform size and shape, small-angle scattering maxima can be observed. The *d* spacings calculated from these SAXS maxima were attributed to the long axis of the crystallites including adjacent amorphous regions connecting the crystallites and were called "long period" (*L*). On the other hand, we can use Scherrer's equation[12] given below to calculate a correlation length L' of crystallites (domains) for semicrystalline polymers from WAXS patterns:

$$L' = \frac{k\lambda}{\beta' \cos\Theta_{max}} \tag{5}$$

Here, k is a material constant, commonly 1 for polymers, λ the wavelength of the X-ray, β' the full width at half-maximum of a WAXS reflection, and Θ_{max} the scattering angle of the reflection under investigation. We are using the 110 reflection in the following, which will give us information about the lateral domain size of the scattering units. This classical approach treats the mesophase structure as a perfect three-dimensional lattice with limited grain sizes and uses approximations from general diffraction relationships.[15]

Results and Discussion

WAXS. When PDES elastomers are uniaxially stretched, a neck forms. Pictures of the neck region taken through crossed polarizers during the transition and after stabilization were published previously.[7] Here, we simply show an illustration in Figure 1 of the stabilized neck under different extension ratios. The sample was mounted in the stretching device and stretched to form a neck. Typical WAXD fiber patterns from a stretched PDES elastomer sample (sample 3) initially and after neck stabilization for about 8 h are shown in Figure 2. Note that the quality and appearance of the X-ray patterns are determined by the mesophase of the PDES that is induced by stretching the sample. Formation of a neck requires some time and depends on temperature, elongation ratio, and characteristics of sample. The kinetics in this experiment was slow enough to follow the neck formation in WAXS and SAXS. Two effects were studied: changes of domain size and *degree of mesophase* with time at fixed locations and variations along the sample in the direction of extension (amorphous−transition−neck). The goal is to answer the question of whether smaller domains are formed that increase in size over time or whether domains of a certain size are formed and the number of these scatterers increases over time. During the experiment, the neck was observed to propagate through the fixed points. The experiment lasted 8 h until the neck stopped propagating and the WAXD pattern did not change noticeably. The WAXD pattern changed gradually with time from an amorphous ring to sharp reflections as expected. Figure 2 shows the WAXD patterns for one fixed point on sample 3 after 25 min and 8 h. The sample was uniaxially stretched in the direction of σ marked in the figure.

The sample-to-film distance has been chosen to show the weak diffuse 111 reflection which reflects three-dimensional order to some degree in the fully stretched, well-aligned samples. The 110 reflection is very strong and consists of amorphous and *mesophase* scattering, depending on the elongation and thermal history. Although the 110 reflection exhibits a rather broad azimuthal arc, a calculation of the orientation parameter reveals values up to 0.9, which is extremely high for an elastomer. (Generally, a nematic phase of a well-aligned liquid crystalline low molecular weight compound shows values up to 0.6.) The broad appearance is a result of the amorphous scattering. The 110 is strong enough to make its second harmonic appear in the pattern, which is a sharp spot toward the beamstop. *d* spacings for the 110 reflections are about 8 Å (see Table 1), which is in agreement with values found in other references.[16,17]

Degree of Mesophase and Mesophase Formation. Figure 3 shows intensities along horizontal line scans through the middle of the X-ray patterns taken from the images as a function of time. A broad peak from scattering of the amorphous region dominates the pattern in the beginning. A sharp mesophase peak emerges at the expense of the broad amorphous peak over time. The two peaks are very close to each other, and at intermediate times the amorphous peak appears as a broad shoulder toward smaller angles of the mesophase peak. The oriented amorphous region has a *d* spacing of 8.1 Å while the mesophase has a *d* spacing of 7.9 Å, consistent with previous studies.

A peak fit of the 2θ scans in Figure 3 allows us to obtain the extent of mesophase formation as the area fraction of the total area that is under the mesophase peak. We assume that very weak scattering from reflections out of this range can be neglected. A sample fit is shown in the inset of Figure 3. The obtained extent of mesophase was further analyzed in terms of the Avrami equation.[18] According to this equation, when a

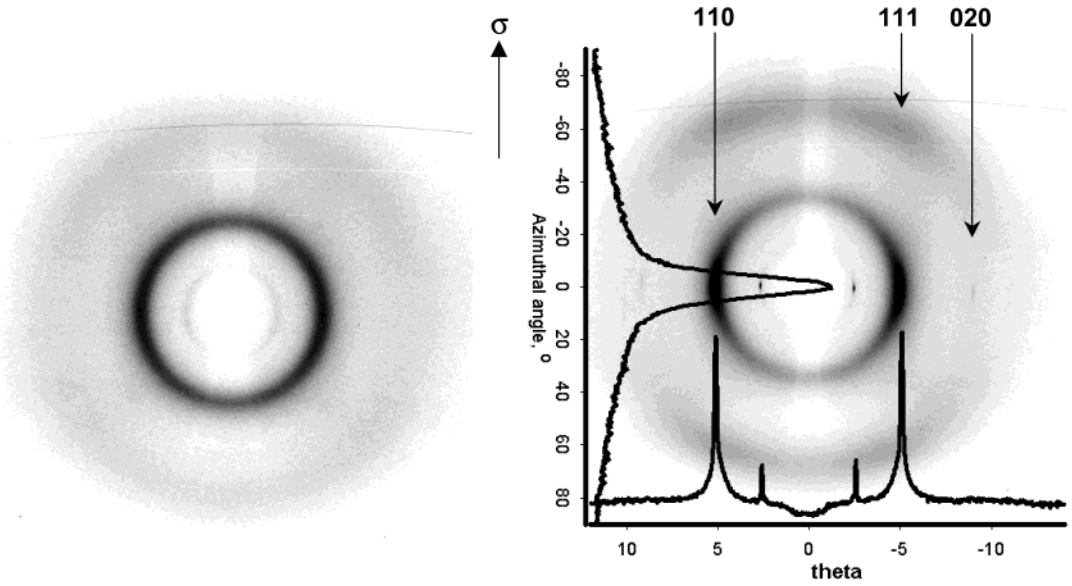

Figure 2. (left) X-ray pattern of amorphous part of sample 3. (right) X-ray pattern of mesomorphic sample 3 after 8 h under constant strain deformation. Also shown are line intensities along the equator and along the azimuth at $\theta = 5°$.

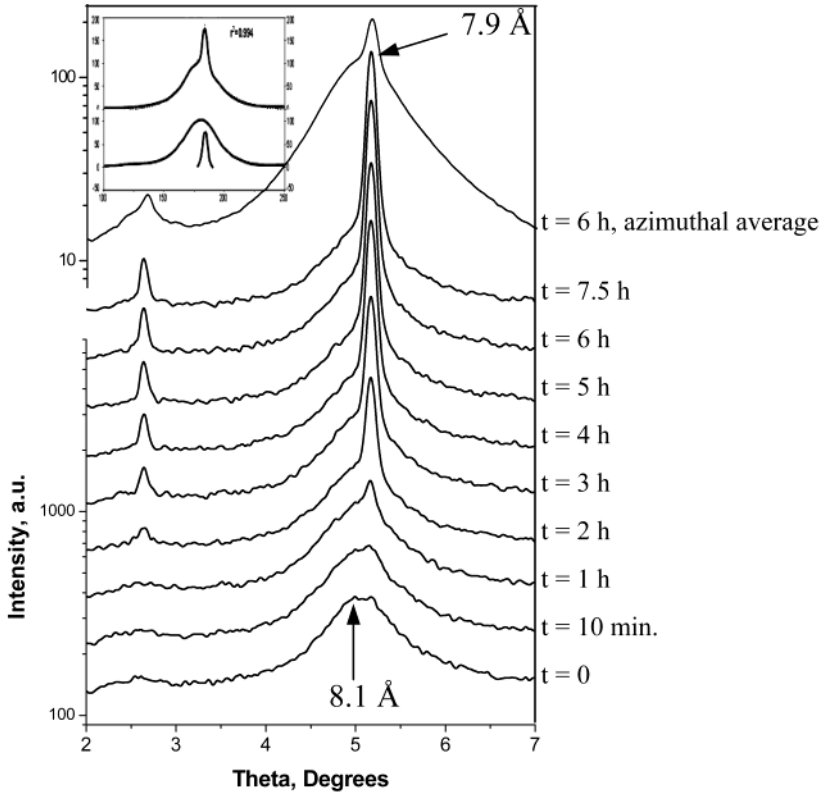

Figure 3. Equatorial line slices from the kinetic study on sample 3. Top curve obtained from azimuthal average. Inset shows fitting procedure for sample 3 at 2 h.

polymer crystallizes from a melt, the degree of crystallinity, C_t %, is related to time, t, in the form of

$$1 - \frac{C_t\%}{C_{\max}\%} = e^{-Zt^n} \qquad (6)$$

where $C_{\max}$% is the maximum crystallinity in the material, Z is the crystallization rate constant containing nucleation and crystal growth rate constants, and n is an integer constant related to the crystallization mechanisms. In particular, $n = 2$ implies either a rod shape or a lamellar shape two-dimensional crystal growth. We shall use this approach here to describe the *condis* crystal mesophase formation of PDES.

Based on the assumption that the integrated intensity of the peak due to the mesophase is directly proportional to the amount of mesophase, a log−log fit of the intensity data using eq 6 yields a slope, i.e., the power n, to be 1.98 (rounded off to 2) as shown in Figure 4. This implies that the mesophase has a two-dimensional shape, either a rodlike shape in the case of thermal nucleation or a lamellar one in the case of athermal nucleation. Optical microscopy observations revealed a lamellar morphology in mesomorphic PDES in previous

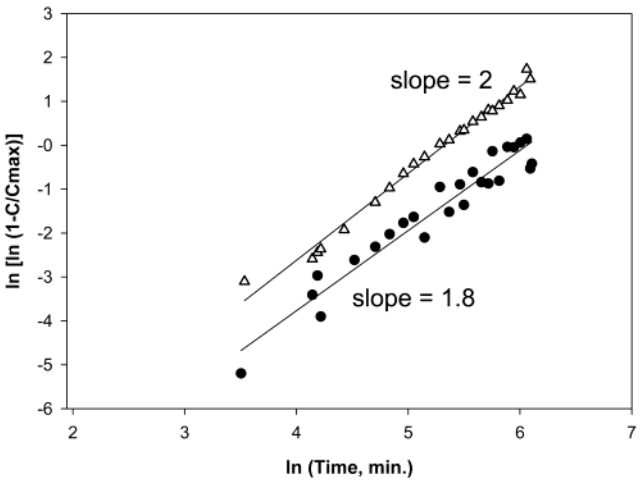

Figure 4. Fitting of Avrami equation for the mesophase formation of sample 3: open triangles from line slice data; filled circles from azimuthal averaged data.

studies.[19] Our WAXS results confirm the kinetics of lamellae formation. Papkov et al. fitted their kinetic results from DSC measurements of PDES mesophase formation to the Avrami equation and obtained a power *n* of about 1.75.[19] If we use azimuthal averaged intensities instead of a line slice along the equator, the results shown in Figure 4 give *a somewhat lower* slope of 1.8. The better agreement with the DSC results is not surprising because we are now also including scattering data from the amorphous direction of the sample (*c*-direction). In other words, a line slice along the equator allows us to monitor the mesophase along one particular direction, and the formation of the mesophase does not necessarily follow the same kinetics in all three dimensions, particularly in a *uniaxially* stretched sample.

Two positions were chosen to study the dynamics of the mesophase formation, one in the neck region (A) and another in the transition region (B) as illustrated in Figure 1. In addition to the orientation parameter and the correlation length, the integrated intensity of the reflections was plotted vs time; the latter gives information about the number of scattering units. As can be seen from Figure 5a−c, the maximum orientation, domain size, and integrated intensity are reached within 100 min for position A, which moves into the neck after a few minutes. Further development of mesophase in position B does not change values in position A. Position B stays in the transition region throughout the experiment, and full orientation is not reached even after 8 h. It can be concluded from the results at position B shown in Figure 5 that domains of a certain size are formed quickly, but the number of domains (intensity plot) only changes gradually. This implies that the mesophase formation starts with domains of about 350 Å, calculated from WAXS data via the Scherrer equation, and the size does not change over the course of crystallization. The more gradual increase in intensity indicates that the number of domains increases as they are formed from material that is being pulled from the amorphous region over time. We discuss below the relation between domain size and the network structure. We note for now that an orientation parameter of 0.85 is extremely high for an elastomer, which is probably due to a very homogeneous distribution of cross-link sites and domains throughout the sample (see Figure 2, azimuthal scan to the left of the X-ray pattern).

SAXS. Calculation of domain sizes from the WAXS pattern via the Scherrer equation assumes a perfect two-phase system and an ideal 3-dimensional packing and may lead to deviations for systems that are more complex such as elastomers with cross-link sites. The calculated value of 350 Å for sample 3 in the previous section is therefore an estimate and is good for comparison to other samples but is not a true representation of domain size (especially since we are using the 110 reflection which reflects the lateral domain dimensions). Sometimes it is possible to obtain domain sizes from a SAXS experiment directly. Limited to constraints in the hutch at the D1 station at CHESS, we used the maximum sample-to-detector distance available to us of 1333 mm. SAXS patterns for sample 2 from the neck region and the transition region are shown in Figure 6. There is a slight tilt of the two-point pattern visible from the transition region, which is due to the curvature of the sample at this point. A *z*-scan through the sample shows that the tilt intensifies as one approaches the curvature of the sample/air interface as one moves in the *z*-direction from point B toward the interface (see Figure 1). *d* spacings for the domain size calculated from the SAXS patterns are listed in Table 1. This domain size here is an average size of the repeat unit consisting of the ordered part as well as the amorphous part of the polymer. There is almost no difference between samples 1 and 2, which should be expected since the molecular weight of the precursor chains and M_c are almost identical.

Results from experiments with sample 4 under partially necked conditions are summarized in Figure 7. They show that the *d* spacing of the domain size changes along the *x*-direction from the amorphous to the mesophase region, $x = 0$ being the transition region. There is a substantial increase from 260 Å in the transition region up to 380 Å in the neck. A further step scan along *x* toward the amorphous region shows that there is little variation in the *d* spacing.

Sample 4 was used to study the effect of the local extension ratio on the structures in the sample. Ink dots were placed on the sample, and digital images were taken of the sample before and after the extension. The local extension ratio was calculated by taking the ratio of the distances before and after stretching between the closest two ink dots that bracket a point of interest. The resulting Figure 8 shows a much larger extension ratio at point A than at point B. Similar to sample 3, points A and B are taken in the neck region and in the transition region, respectively. The increasing *d* spacing of point B with increasing extension indicates that the domains grew with increasing strain. Point A located within the neck region has practically constant *d* spacing, indicating that the size of mesophase domains within the neck was independent of the local extension ratio when α exceeded 3.2. In a partially necked PDES sample, the SAXS *d* spacing increases with increasing local extension ratio as demonstrated in Figure 8. As the local extension ratio increased above 3.3, the increase in *d* spacing, and hence the distance between domains, including the amorpous part, reached saturation. The results in Figure 7 reflect therefore the local extension ratio in the samples considered.

The extent of orientation calculated from the SAXS experiment via eqs 2−4 agrees very well with that calculated from the WAXS experiment and confirms the high value of 0.85 for the order parameter in this

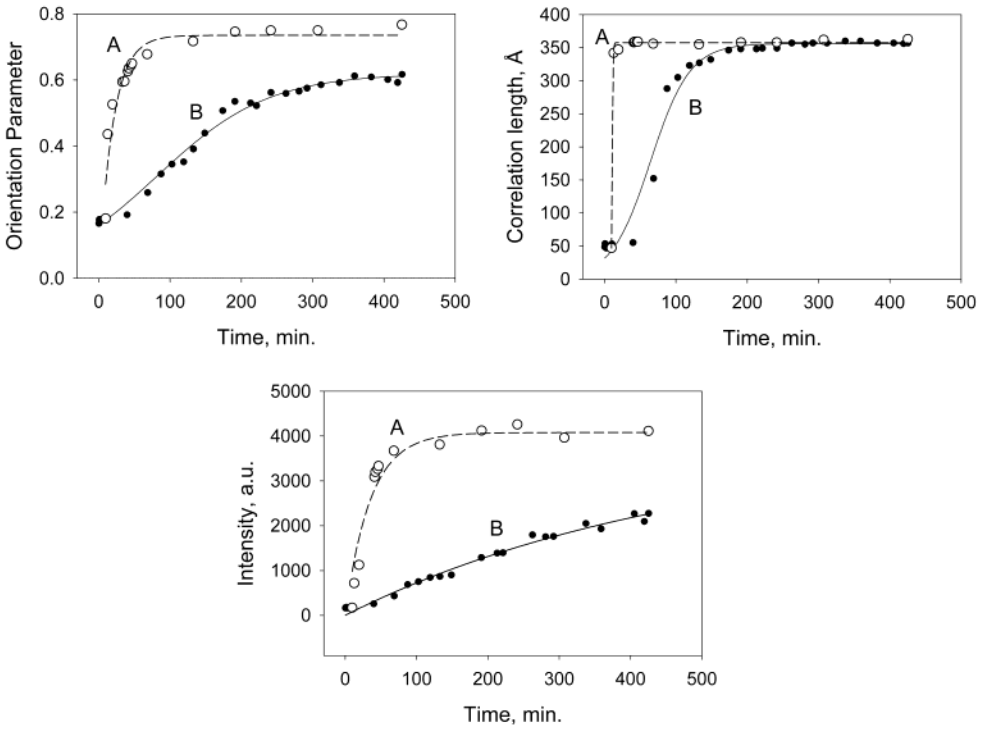

Figure 5. Mesophase formation for sample 3 for positions A and B: (a) orientation parameter, (b) correlation length, (c) intensity.

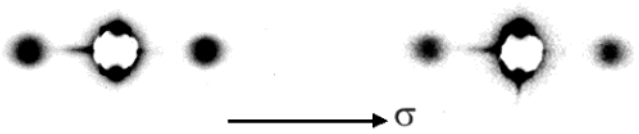

Figure 6. SAXS patterns of sample 2 in the neck (left) and the transition region (right). A slight tilt can be seen in the transition region.

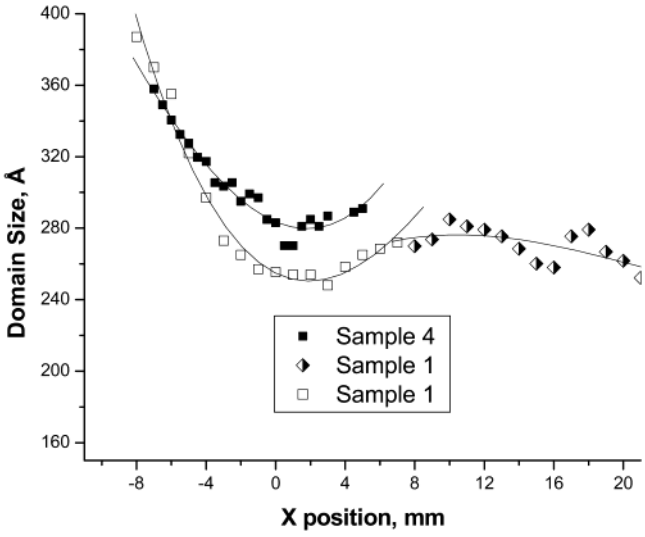

Figure 7. Step scan along stretching direction for samples 1 and 4.

elastomer. SAXS *d* spacing in the fully necked samples 1 and 2 is about 270 Å, whereas it reaches 380 Å in the partially necked sample 4. The main difference between these samples is the number-average molecular weight of the precursor chains forming the end-linked network. Samples 1 and 2 were formed from precursors of about 20 kg/mol whereas sample 4 was formed from precursors of 34.5 kg/mol. It indicated that the polymer chains near the cross-link points could not form a mesophase

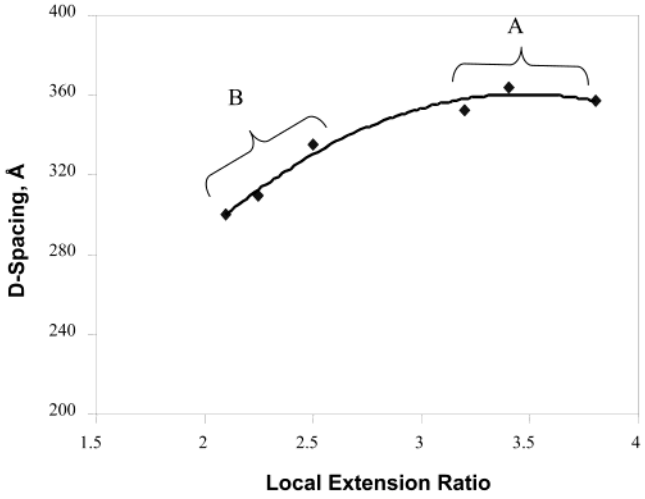

Figure 8. Domain size vs local extension ratio for sample 4.

due to a starlike structure. As a result, longer precursor chains allow for the formation of larger domains. Sample 3 with a precursor molecular weight of 26 kg/mol results in a domain size in the neck region of almost 300 Å and fits well in the postulated correlation between molecular weight and domain size (Figure 9). Note that the absolute value of domain size observed in the SAXS is smaller than the value calculated from the WAXS pattern via the Scherrer equation for sample 3, which is due to assumtpions made in the model and geometry. It is obvious from this plot that domain size does not depend on the molecular weight between effective cross-links given by M_c and obtained from the equilibrium elastic modulus of the network that takes into account trapped entanglements. The latter contribute to the value of the equilibrium elastic modulus[10] but do not play a role in the size of the mesophase domains formed here. This is consistent with recent Monte Carlo simulations that indicate that in uniaxial extension the

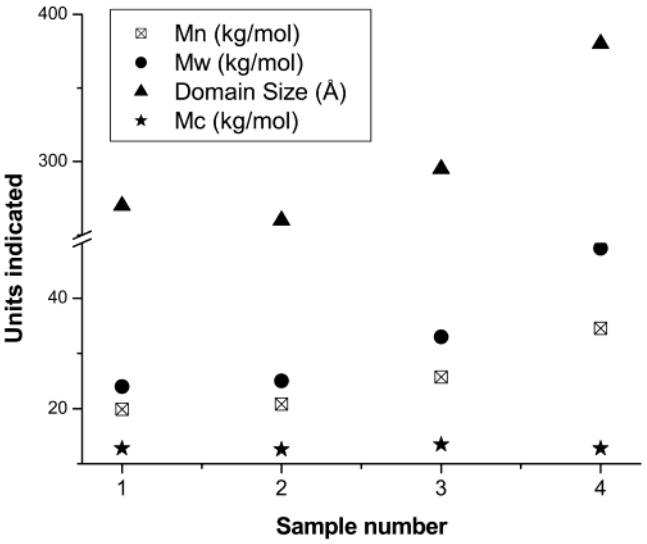

Figure 9. Trends: in molar mass of precursor chains (M_n and M_w), in molar mass between effective cross-links (M_c) calculated from the equilibrium modulus, and in domain size.

effects of trapped entanglements are important at small deformations (such as in the value of the equilibrium elastic modulus) but become less important at high deformation because of entanglement slippage.[20]

Conclusions

The X-ray results obtained here are consistent and complement previous deuterium NMR studies.[7] The D-NMR peak splitting of the mesophase in the neck region remained constant at 19 kHz as a function of extension ratio, indicating that the orientation parameter does not change in the mesophase as a function of extension. X-ray measurements allowed for a quantitative measurement of the order parameter. Once a full neck was achieved, an increase in degree of mesophase with increase in extension ratio was observed by NMR, and it was concluded that amorphous material in the neck was converted into the mesophase. The present X-ray results enable us to determine that the increase in the extent of mesophase is due to an increase in the number of the domains and not in their size. Furthermore, we find that the size of the domains remains constant in the neck as a function of extension ratio (data of point A in Figure 8) and that the size of the domains is governed by the size of the precursor chains used in the end-linking. The measured size of the mesophase domains correlates well with the average size of the precursor chain between covalent cross-links (Figure 9). This result was hinted at qualitatively on the basis of the D-NMR study as the samples with the highest degree of chemical cross-linking led to the lowest mesophase content. The samples with the highest molar mass of their precursors yielded the highest extent of mesophase content.

Acknowledgment. We thank D. Foti for writing the routine for the analysis of the X-ray diffraction patterns under Matlab. We also thank a reviewer for valuable input. Financial support from the National Science Foundation, Division of Materials Research and Polymers Program Grant DMR-0078863, is gratefully acknowledged. This work is based upon research conducted at the Cornell High Energy Synchrotron Source (CHESS) which is supported by the National Science Foundation and the National Institutes of Health/ National Institute of General Medical Sciences under Award DMR 9713424.

References and Notes

(1) Godovsky, Y. K. *Angew. Makromol. Chem.* **1992**, *202/203*, 187.
(2) De Gennes, P. G.; Herbert, M.; Kant, R. *Macromol. Symp.* **1997**, *113*, 39.
(3) Miller, K. J.; Grebowicz, J.; Wesson, J. P.; Wünderlich, B. *Macromolecules* **1990**, *23*, 849.
(4) Ran, S.; Zong, X.; Fang, D.; Hsiao, B. S.; Chu, B. *Macromolecules* **2001**, *34*, 2569.
(5) Wünderlich, B.; Grebowicz, J. *Adv. Polym. Sci.* **1984**, *60/61*, 1.
(6) Hedden, R. C.; Saxena, H.; Cohen, C. *Macromolecules* **2000**, *33*, 8676.
(7) Hedden, R. C.; Tachibana, H.; Duncan, T. M.; Cohen, C. *Macromolecules* **2001**, *34*, 5540.
(8) Tsvankin, D. Y.; Papakov, V. S.; Zhukov, V. P.; Godovsky, Y. K. *J. Polym. Sci., Polym. Chem. Ed.* **1985**, *23*, 1043.
(9) Out, G.; Turetskii, A. A.; Snijder, M.; Möller, M.; Papkov, V. S. *Polymer* **1993**, *36*, 3213.
(10) Patel, S. K.; Malone, S.; Cohen, C.; Gillmor, J.; Colby, R. H. *Macromolecules* **1992**, *25*, 5241.
(11) Hedden, R. C.; McCaskey, E. F.; Cohen, C.; Duncan, T. M. *Macromolecules* **2001**, *34*, 3285.
(12) Kakudo, M.; Kasai, N. *X-ray Diffraction by Polymers*; American Elsevier Publishing Co., Inc.: New York, 1972.
(13) Alexander, L. E. *X-ray Diffraction Methods in Polymer Science*; Robert E. Kereger Publishing Co.: New York, 1979.
(14) Hosemann, R.; Hindeleh, A. M. *J. Macromol. Sci., Phys.* **1995**, *B34*, 327.
(15) Tsukruk, V. V.; Shilov, V. V. *Polymer* **1990**, *31*, 1793. See also: Tsukruk, V. V.; Bunning, T. J.; Koerner, H.; Ober, C. K.; Adams, W. W. *Macromolecules* **1996**, *29*, 8706.
(16) Godovsky, Y. K.; Slonimsky, G. L. *J. Polym. Sci., Polym. Phys. Ed.* **1974**, *12*, 1053.
(17) Inomata, K.; Yamamoto, K.; Nose, T. *Polym. J. (Tokyo)* **2000**, *32*, 1044.
(18) Avrami, M. *J. Chem. Phys.* **1939**, *7*, 1103.
(19) Papkov, V. S.; Svistunov, V. S.; Godovsky, Yu. K.; Zhdanov, A. A. *J. Polym. Sci., Part B: Polym. Phys.* **1987**, *25*, 1859.
(20) Chen, Z.; Cohen, C.; Escobedo, F. *Macromolecules* **2002**, *35*, 3296.

MA020856J